Multicritical Phase Diagram of Gases Adsorbed on Graphite: Temperature Variation and Finite-Size Effects

S. Ostlund and A. N. Berker
Department of Physics, Harvard University, Cambridge, Massachusetts 02138
(Received 6 October 1978)

Multicritical phase diagrams for krypton and nitrogen submonolayers adsorbed on graphite are calculated from a position-space renormalization, with flows in a 22-parameter space. Quantitative agreement with experiment is excellent, with no adjustable parameter. Temperature variation and finite-size effects are taken into account, causing a cusped coexistence boundary at the multicritical point. Incipient liquid-gas criticality is derived.

Phase transitions in submonolayers on graphite are of much interest.[1-14] The hexagonal basal (001) surface of graphite presents a periodic substrate. The centers of the hexagons are preferred adsorption sites and form a triangular lattice. The potential between krypton or nitrogen adatoms forbids the simultaneous occupation of nearest-neighbor sites, whereas further-neighbor occupation is favorable. We report here a renormalization[12] calculation which starts from the microscopic description of adsorbed krypton and nitrogen, and yields, with no adjustable parameter, excellent quantitative agreement with experimentally observed[1-10] multicritical phase diagrams (Figs. 1 and 2). Temperature variation and finite-size[15] effects of experimental systems are taken into account, causing a cusped coexistence boundary suggested by experiments.[1,2,5,8-10] Our calculation derives incipient liquid-gas criticality.[16]

A "solid" ($\sqrt{3}\times\sqrt{3}$ epitaxial) phase, with preferential occupation of one of three sublattices, is distinguished from a "fluid" phase with equivalent occupation of each sublattice. These are separated by a line of higher-order transitions and, at low temperatures, by a first-order coexistence region (Fig. 3, full curves). The higher-order line joins the convex coexistence region at a multicritical[13] point. As the multicritical temperature T_B is approached, the coexisting densities approach each other as $(T_B - T)^{\beta_u}$. The exponent β_u is 0.206 in this calculation, as determined by the multicritical fixed point. Without taking this value too quantitatively, note that it is less than 1, which gives the flat coexistence boundary near T_B.

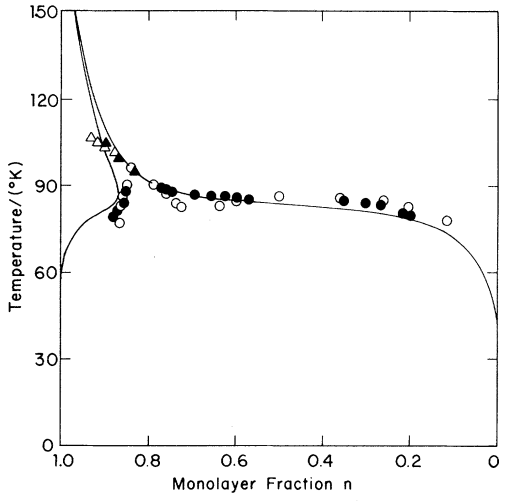

FIG. 1. Predicted phase diagram for krypton on graphite, with smearing $\Delta T = 0.8$ K. Phase boundary points from experiments are as follows: first-order transitions from Refs. 1 (open circles) and 2 (closed circles); higher-order transitions from Refs. 1 (open triangles) and 3 (closed triangles). The density scale of Ref. 2 is determined by adjusting the high-density points to Ref. 1.

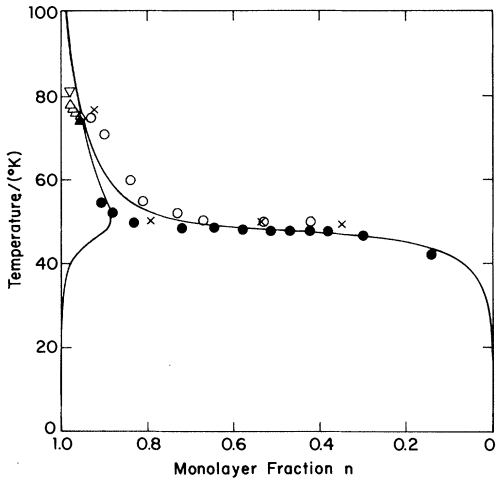

FIG. 2. Predicted phase diagram for nitrogen on graphite, with smearing $\Delta T = 0.8$ K. Phase boundary points from experiments are as follows: first-order transitions from Refs. 6 (crosses), 8 (closed circles), and 9 (open circles); higher-order transitions from Refs. 7 (open triangles), 8 (closed triangle), and 9 (inverted triangle).

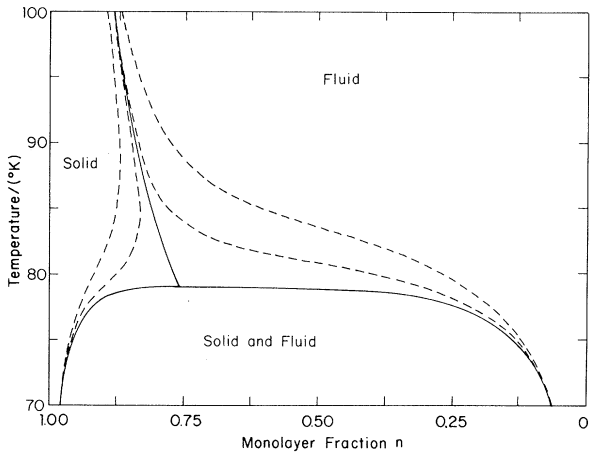

FIG. 3. Temperature variation and finite-size effects on the multicritical region for krypton on graphite. Full curves correspond to the ideal thermodynamic system ($\Delta T = 0$). Dashed curves were calculated with temperature smearings of $\Delta T = 0.1$ and 0.8 K.

The above description applies to a thermodynamic (infinite-extent) system which has equilibrated under uniform conditions. Even for this idealized case, we had to keep an accuracy of 1 part in 10^{10} in temperature and chemical potential to obtain the full curves in Fig. 3. This is somewhat removed from the experimental situation. Because of temperature nonuniformities and variations during a single measurement at uniform pressure, a small interval ΔT in temperature is actually sampled. If the graphite came as a tightly packed powder, percolative effects would cause variations in pressure as well. The finite size of graphite crystallites has a similar effect. As the higher-order transition temperature T_c is approached, the correlation length ξ diverges as $\xi_0|(T - T_c)/T_c|^{-\nu}$, where ξ_0 is expected to be of the order of the range of the couplings. The transition is smeared[15] within a temperature interval ΔT in which ξ for the ideal system would surpass the characteristic crystallite size L, so that $L = \xi_0(\Delta T/2T_c)^{-\nu}$. The overall temperature smearing ΔT depends on substrate, experimental setup, pressure, and average temperature. We used $\Delta T = 0.8$ K, suggested by a recent experiment.[5] Quantitative changes described below appear mainly as ΔT varies between the ideal zero and about 0.2 K.

We have taken into account temperature variation and finite-size effects by incorporating into the evaluation of densities a temperature smearing of ΔT. First, the phase boundary lines in temperature–chemical-potential space were determined accurately. Then, densities were evaluated in the range $\pm\Delta T/2$ from these lines, at given[17] chemical potential μ. When this was carried out, the higher-order transition occurred over a range of densities, observable close to the multicritical point. This portion of the phase diagram thus became a narrow continuation of the coexistence region (Fig. 3, dashed curves), yielding the *cusped coexistence boundary* suggested by experiments.[1,2,5,8-10] These effects are important because the density n varies sharply[14] at the higher-order transition, as $|n - n_c| \sim |T - T_c|^{1-\alpha}$. The appropriate[11] three-state Potts-model exponent[18] is $1 - \alpha \sim 0.6$. The effective value for this exponent gets much smaller as the multicritical point is approached, because of crossover to the multicritical form[19] $1 - \alpha_B = 0.067$. In addition to modifying the shape of the apparent coexistence region as estimated by our temperature-smearing procedure, nonideal effects will of course round the thermodynamic signals at the dashed boundaries in Fig. 3.

Predicted phase diagrams for krypton and nitrogen submonolayers are in Figs. 1 and 2. Experimental data[1-3,6-9] are also shown. The quantitative agreement is excellent, with no adjustable parameter. Larher[10] has observed, for nitrogen on graphite, a very narrow coexistence region which shifted to higher density as it stretched up to 82 K. This is reproduced by our bending cusp in Fig. 2. Our phase diagrams exhibit a single fluid phase. However, note the nearly horizontal boundary between the fluid and the coexistence region. Within trajectories which flow close to a liquid-gas critical fixed point a small change in initial conditions would introduce a liquid-gas critical point. This "incipient criticality" mechanism, proposed by Griffiths,[16] explains the experimentally observed specific-heat maxima.[4,8] This region is very close, in temperature and chemical potential, to the multicritical point. Thus, another explanation is that a given experimental measurement at the near-horizontal boundary actually samples the multicritical region, because of the ΔT effects discussed above.

Our calculations start from adatoms interacting pairwise via a Lennard-Jones potential $V(r) = 4\epsilon[(\sigma/r)^{12} - (\sigma/r)^6]$. The renormalization is applied to the lattice-gas Hamiltonian,

$$\mathcal{H} = -\sum_m \sum_{(ij)_m} J^{(m)} n_i n_j - \mu \sum_i n_i, \qquad (1)$$

where $n_i = 0$ (1) when graphite site i is empty

(full), and $\langle ij\rangle_m$ represents an mth-neighbor pair of sites. At full registered monolayer coverage, every second neighbor of an occupied site is also occupied. The solid phase ($n > 0.87$) is always close to full coverage ($n = 1$). Accordingly, a temperature-dependent second-neighbor coupling constant is derived from the simple coarse-graining formula

$$J^{(2)} = z^{-2} \int d^2r_i\, d^2r_j\, V(|\vec{r}_i - \vec{r}_j|) \exp\{-[U(\vec{r}_i) + U(\vec{r}_j)]/kT\}, \tag{2}$$

with $z = \int d^2r \exp\{-U(\vec{r})/kT\}$. The integrals in (2) are over the two hexagons $\langle ij\rangle_2$. The integral in z is over one hexagon. $U(\vec{r})$ is the sum of the substrate potential,

$$U_s(\vec{r}) = \tfrac{2}{9} U_0 \{\cos(\vec{a}_1 \cdot \vec{r}) + \cos(\vec{a}_2 \cdot \vec{r}) + \cos[(\vec{a}_1 + \vec{a}_2) \cdot \vec{r}]\}$$

where $\vec{a}_{1,2}$ are the reciprocal-lattice vectors, and of the potential caused by the occupation of all six second-neighbor sites. At full monolayer coverage, no third- or fourth-neighbor pair of sites are simultaneously occupied. Thus, the phase diagram depends only weakly on $J^{(3)}$ and $J^{(4)}$. No reasonable coarse-graining formula presents itself for these constants, so the values of $V(r)$ at the corresponding site separations are taken. We use the substrate[20] well depth $U_0 = 37$ K, and the Lennard-Jones parameters $\epsilon = 145$ and 78 K and $\sigma = 3.60$ and 3.70 Å for krypton[3] and nitrogen, respectively.[14] (The first-neighbor site separation is 2.46 Å.) A lattice gas results, with first-neighbor occupation forbidden, and further-neighbor occupation favored, but decreasingly with separation. The $m \geq 5$ couplings are negligible.

Nearest-neighbor exclusion allows us to group the lattice-gas *sites* into triplets [Fig. 4(a)] and to associate a *spin* which either points from the center of the triplet toward an occupied site, or is zero meaning no occupation. The lattice-gas Hamiltonian (1) then determines a nearest-neighbor spin Hamiltonian, with spin degrees of freedom coupled to the lattice directions. This includes most of the original lattice-gas interactions, i.e., all of the first-neighbor exclusions, all of the second-neighbor interactions, and $\frac{2}{3}$ and $\frac{1}{3}$ of the third- and fourth-neighbor interactions. The spin interactions belong to every other adjacent spin triplet [Fig. 4(b)]. Such an interacting spin triplet is called a *plaquette*. The renormalization is applied[19] to the plaquette system.[21] In a 2×2 unit cell, one plaquette is moved[22] onto the other three [Fig. 4(c)], and the interior spins are dedecorated [Fig. 4(d)]. Renormalization-group trajectories are generated in the 22-dimensional space of the most general spin-triplet Hamiltonian,

$$-\mathcal{H}/kT = \sum_P \sum_c K^{(c)} Q^{(c)}(\vec{s}_{1P}, \vec{s}_{2P}, \vec{s}_{3P}), \tag{3}$$

where P denotes a plaquette, and c denotes a configuration of the spins $\vec{s}_{1P}$, $\vec{s}_{2P}$, $\vec{s}_{3P}$. The projection operator $Q^{(c)}(\vec{s}_1, \vec{s}_2, \vec{s}_3)$ is 1 (0) when $\vec{s}_1$, $\vec{s}_2$, $\vec{s}_3$ are (are not) in configuration c. Many configurations map onto each other by the symmetries of the triangle and have identical interaction constant $K^{(c)}$, which reduces the number of distinct $K^{(c)}$ from 64 to 22. This procedure is sensitive to the connectivity of the lattice gas, and thus takes into account "frustration" effects occurring when the lattice geometry is incompatible with every bond having lowest energy.

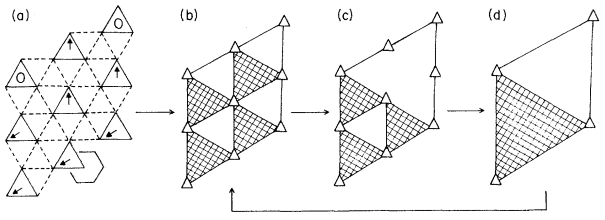

FIG. 4. Prefacing and renormalization procedures. In (a), a spin configuration and one basal graphite hexagon is shown. In (b), (c), and (d), small triangles represent spins, and cross-marked triangles represent plaquettes.

We are grateful to B. I. Halperin and D. R. Nelson for critically reading our manuscript, and to R. J. Birgeneau, D. M. Butler, R. B. Griffiths, E. M. Hammonds, P. Heiney, P. M. Horn, F. A. Putnam, and G. A. Stewart for useful conversations. This work was in part supported by the National Science Foundation under Grant No. DMR77-10210 and (for A.N.B.) an IBM Postdoctoral Fellowship.

[1]A. Thomy and X. Duval, J. Chim. Phys. 66, 1966 (1969), and 67, 286, 1101 (1970).

[2]Y. Larher, J. Chem. Soc. Faraday Trans. I 70, 320 (1974).

[3]F. A. Putnam and T. Fort, Jr., J. Phys. Chem. 79, 459 (1975), and 81, 2164 (1977); F. A. Putnam, T. Fort, Jr., and R. B. Griffiths, J. Phys. Chem. 81, 2171

(1977).
[4]D. Butler, J. A. Litzinger, and G. A. Stewart, Bull. Am. Phys. Soc. 23, 565 (1978), and to be published.
[5]P. M. Horn, R. J. Birgeneau, P. Heiney, and E. M. Hammonds, Phys. Rev. Lett. 41, 961 (1978).
[6]J. K. Kjems, L. Passell, H. Taub, and J. G. Dash, Phys. Rev. Lett. 32, 724 (1974); J. K. Kjems, L. Passell, H. Taub, J. G. Dash, and A. D. Novaco, Phys. Rev. B 13, 1446 (1976).
[7]D. M. Butler, G. B. Huff, R. W. Toth, and G. A. Stewart, Phys. Rev. Lett. 35, 1718 (1975).
[8]T. T. Chung and J. G. Dash, Surf. Sci. 66, 559 (1977).
[9]W. F. Brooks, Ph.D. thesis, Stevens Institute of Technology, 1977 (unpublished); W. F. Brooks, W. D. Ellenson, and L. Passell, to be published.
[10]Y. Larher, J. Chem. Phys. 68, 2257 (1978).
[11]S. Alexander, Phys. Lett. 54A, 353 (1975).
[12]M. Schick, J. S. Walker, and M. Wortis [Phys. Lett. A58, 479 (1976), and Phys. Rev. B 16, 2205 (1977)] have applied the renormalization approach to the higher-order transition of helium on graphite.
[13]The Monte Carlo study by B. Mihura and D. P. Landau [Phys. Rev. Lett. 38, 977 (1977)] yielded a multicritical phase diagram for a triangular-lattice model.
[14]A. N. Berker, S. Ostlund, and F. A. Putnam, Phys. Rev. B 17, 3650 (1978).
[15]M. E. Fisher and A. E. Ferdinand, Phys. Rev. Lett. 19, 169 (1967); A. E. Ferdinand and M. E. Fisher, Phys. Rev. 185, 832 (1969).
[16]R. B. Griffiths, private communication.
[17]Since, in a fixed-pressure experiment, μ is a function of T, a more proper procedure would also include a variation $\Delta\mu$. We checked that this does not significantly affect our results, and that chemical-potential smearing is equivalent to temperature smearing.
[18]T. de Neef and I. G. Enting, J. Phys. A 10, 801 (1977).
[19]S. Ostlund and A. N. Berker, to be published.
[20]The values $U_0 = 37$ and 35 K are given for krypton and xenon, respectively, on graphite by G. L. Price and J. A. Venables, Surf. Sci. 59, 509 (1976). Our results are very weakly dependent on this parameter.
[21]I. G. Enting [Aust. J. Phys. 31, 383 (1978)] has investigated a similar system using series expansions.
[22]A. A. Migdal, Zh. Eksp. Teor. Fiz. 69, 1457 (1975) [Sov. Phys. JETP 42, 743 (1976)]; L. P. Kadanoff, Ann. Phys. (N.Y.) 100, 359 (1976), and Rev. Mod. Phys. 49, 267 (1977).

Theory of the Heats of Formation of Transition-Metal Alloys

D. G. Pettifor[a]
Bell Laboratories, Murray Hill, New Jersey 07974
(Received 10 August 1978)

A simple expression for the heat of formation ΔH of transition-metal alloys is derived within the tight-binding approximation that has the form $\Delta H = f(\bar{N})\Delta N^2$, where $\bar{N}$ and ΔN are the average and difference in number of valence d electrons, respectively. The prefactor $f(\bar{N})$ is most negative for $\bar{N}$ lying near the middle of the series and it becomes positive towards the edges. The theory gives good agreement with Miedema's semiempirical values of ΔH.

Recently Boom, de Boer, and Miedema[1] have developed a highly successful semiempirical scheme that reporduces the observed signs of the heat of formation of about 500 alloys of the simple and transition metals. It is a natural extension of Pauling's[2] original description of electronegativity in which the heat of formation ΔH was proposed to be proportional to the square of the electronegativity difference ΔX. Boom, de Boer, and Miedema,[1] in order to overcome the problem that Pauling's scheme always predicts a negative ΔH, included a repulsive contribution proportional to the square of the charge-density mismatch at the Wigner-Seitz boundary $\Delta N^{1/3}$. Thus

$$\Delta H_{\text{Miedema}} = -P(\Delta\varphi^*)^2 + Q(\Delta n^{1/3})^2, \qquad (1)$$

where the attractive charge-transfer term was originally[3] assumed proportional to the square of the difference in the work function $\Delta\varphi$. Unfortunately, good agreement with the experimental sign of ΔH could only be achieved by adjusting the experimental work function φ, sometimes by as much as $\Delta\varphi$ itself, to new values[1] φ^*. It was, therefore, not clear what fundamental significance should be attached to the final coordinate φ^*. In this Letter a microscopic theory of the heat of formation of transition-metal alloys will be presented that not only gives good agreement without any adjustable parameters to Miedema's semiempirical values of ΔH, but also suggests a different interpretation of the underlying physics of the coordinate φ^* from that previously[1] ascribed to it.

The cohesive energy of the pure transition-metal constituents arises[4,5] from the strong bonding of the valence d electrons, which are well de-